



**HAL**  
open science

## **Cyclodextrins: a new and effective class of co-modulators for aqueous zirconium-MOF syntheses**

Guillaume Hoyez, Jolanta Rousseau, Cyril Rousseau, Sébastien Saitzek, James King, Petra Ágota Szilágyi, Christophe Volkringer, Thierry Loiseau, Frédéric Hapiot, Eric Monflier, et al.

### ► To cite this version:

Guillaume Hoyez, Jolanta Rousseau, Cyril Rousseau, Sébastien Saitzek, James King, et al.. Cyclodextrins: a new and effective class of co-modulators for aqueous zirconium-MOF syntheses. *CrystEngComm*, 2021, 23 (14), pp.2764-2772. 10.1039/D1CE00128K . hal-03199014

**HAL Id: hal-03199014**

**<https://hal.science/hal-03199014>**

Submitted on 22 Nov 2023

**HAL** is a multi-disciplinary open access archive for the deposit and dissemination of scientific research documents, whether they are published or not. The documents may come from teaching and research institutions in France or abroad, or from public or private research centers.

L'archive ouverte pluridisciplinaire **HAL**, est destinée au dépôt et à la diffusion de documents scientifiques de niveau recherche, publiés ou non, émanant des établissements d'enseignement et de recherche français ou étrangers, des laboratoires publics ou privés.

# Cyclodextrins: a New and Effective Class of Co-Modulators for Aqueous Zirconium-MOF Syntheses

Guillaume Hoyez,<sup>a</sup> Jolanta Rousseau,<sup>a</sup> Cyril Rousseau,<sup>a</sup> Sébastien Saitzek,<sup>a</sup> James King,<sup>b</sup> Petra Ágota Szilágyi,<sup>b</sup> Christophe Volkringer,<sup>c</sup> Thierry Loiseau,<sup>c</sup> Frédéric Hapiot,<sup>a</sup> Eric Monflier,<sup>a</sup> and Anne Ponchel<sup>\*a</sup>

Inspired by the effectiveness of cyclodextrin (CD) auxiliary agents in the design of nanocomposite materials, we hypothesized that the same approach can be employed in the controlled assembly of zirconium-based Metal-Organic Frameworks (Zr-MOFs) of the UiO-66-X topology, in aqueous media. Native CDs ( $\alpha$ -CD,  $\beta$ -CD and  $\gamma$ -CD) in different proportions were initially applied as co-modulators to the reaction mixture of the  $Zr_6O_4(OH)_4(CH_3COOH)_{12}$  cluster zirconium precursor and the 2-aminoterephthalic acid linker, to assess their influence on the porous properties of the Zr-MOFs. Crystallinity and textural characteristics of the so-obtained materials were determined by mean of X-ray diffraction and  $N_2$ -sorption analysis. Even at low concentrations,  $\gamma$ -CD was shown to have a deleterious effect on the Zr-MOFs' specific surface area and their overall  $N_2$  sorption properties. Conversely,  $\alpha$ -CD and  $\beta$ -CD aided synthesis of Zr-MOFs resulted in superior textural properties outperforming those obtained with classical hydrothermal syntheses, yielding a record surface area of  $S_{BET} = 1451 \text{ m}^2\cdot\text{g}^{-1}$ , suggesting that these co-modulators efficiently participate in the growth of UiO-66-NH<sub>2</sub>. This effect is hereby rationalized through the different roles played by the CDs towards the reagents in the UiO-66-NH<sub>2</sub> reaction mixture, and a reaction mechanism is proposed.

## Introduction

Metal-organic frameworks (MOFs) have attracted much attention during the past decade as they exhibit great potential in many applications such as gas storage, drug delivery, catalysis, separation, imaging and sensing. MOFs consists of crystalline networks resulting from coordination of polytopic organic linkers onto oxo/hydroxo clusters.<sup>1,2</sup> Their applicability in catalysis has now been amply demonstrated,<sup>3,4,5,6</sup> and their effectiveness is greatly dependent on their specific surface area (SSA) and presence of defects within the MOF network.<sup>7,8,9,10,11</sup> Since the seminal works by Schaate et al. in 2011,<sup>12</sup> it has been assumed that modulators mainly allow adjusting reaction kinetics of the nucleation and the growth of MOFs, however, they also alter the regular arrangement of their constitutive oxo/hydroxo clusters and polytopic organic linkers to create defects, e.g. missing linkers or missing nodes.<sup>13,14</sup> Modulators are typically non-bridging ligands, which compete with linkers by coordination to the metal clusters.<sup>15</sup> So far, monocarboxylic acids such as benzoic, formic, acetic and trifluoroacetic acid are amongst the most employed. The number of defects in the MOF lattices is strongly correlated with the steric hindrance, the concentration and/or acidity of the modulator.<sup>16</sup> Small quantities of modulators prevent the formation of the kinetically preferred disordered MOFs, the reason for this is that coordination equilibria between metal clusters, linkers and modulators regulate the rate of crystal growth and therefore the framework extension. Such exchange processes lead to the controlled growth of phase-pure crystalline frameworks that otherwise would only result in the formation of an amorphous

powder.<sup>17</sup> Conversely, large modulator concentrations result in the formation of highly defective MOFs.<sup>18</sup> Vacancy concentrations can be controlled in a systematic manner, as shown by Cliffe et al.<sup>19</sup>

Herein, we propose an innovative strategy to influence the crystal growth of Zr-MOFs using a saccharide-based modulator. Specifically, we have set out to systematically investigate the effect saccharides play in altering the Zr-MOF formation in conjunction with monocarboxylate acid modulators. One might expect that the MOF structure at the nanoscale might be affected by the coordination of saccharide hydroxyl groups to the Zr-node. To validate our hypothesis, we selected the benchmark MOF UiO-66-NH<sub>2</sub> as the model.<sup>20,21</sup> UiO-66-NH<sub>2</sub> is a zirconium-based metal-organic framework, which consists of  $[Zr_6O_4(OH)_4]^{12+}$  secondary building units (SBU) linked together by 2-aminoterephthalate carboxylates (BDC-NH<sub>2</sub>) (Figure 1).

To our knowledge, nothing has been described so far on the utilization of saccharides as co-modulators to tune the structure of UiO-66-NH<sub>2</sub>. In line with this, we attempted the hydrothermal synthesis of UiO-66-NH<sub>2</sub> in the presence of both acetic acid and saccharides. We especially compared the ability of two acyclic saccharides –sorbitol and  $\alpha$ -D-methyl glucopyranose– and three cyclic oligosaccharides – $\alpha$ -,  $\beta$ - and  $\gamma$ -cyclodextrins (CD)– to alter the UiO-66 morphological and structural properties across a range of concentrations. Through a detailed analysis of the MOF structures obtained in each case, we demonstrate that it is possible to synthetically control the specific surface area (SSA) and porosity of the UiO-66-NH<sub>2</sub> crystallites through a judicious choice of saccharides

<sup>a</sup> Univ. Artois, CNRS, Centrale Lille, Univ. Lille, UMR 8181 – UCCS – Unité de Catalyse et Chimie du Solide, F-62300 Lens, France.

<sup>b</sup> Queen Mary University of London, School of Engineering and Materials Science, Mile End Road, E1 4NS London, UK.

<sup>c</sup> Univ. Lille, CNRS, Centrale Lille, Univ. Artois, UMR 8181 – UCCS – Unité de Catalyse et Chimie du Solide, F-59000 Lille, France.

Electronic Supplementary Information (ESI) available: Materials and methods, MOF formulas, textural properties, XRD patterns, FTIR and NMR spectra, CO<sub>2</sub> sorption isotherms, N<sub>2</sub> sorption isotherms, DSC, TEM, dispersion.

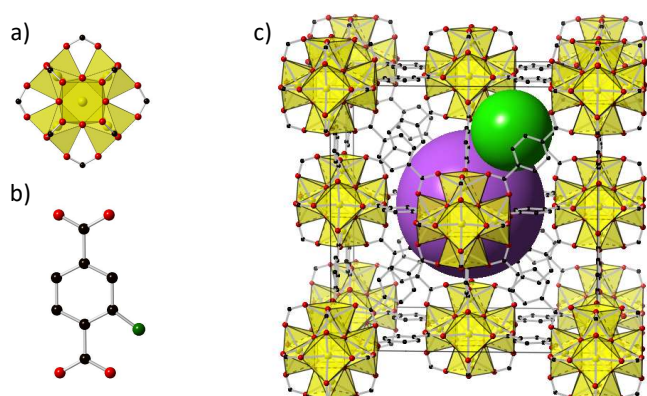


Fig 1. Schematic structural illustration of UiO-66-NH<sub>2</sub>. a) [Zr<sub>6</sub>O<sub>4</sub>(OH)<sub>4</sub>]<sup>12+</sup> cluster as secondary building unit (SBU), b) 2-aminoterephthalate carboxylate (BDC-NH<sub>2</sub>) as an organic linker, and c) the face-centred-cubic (fcc) crystal structure of UiO-66-NH<sub>2</sub>. Purple sphere: octahedral cavity; green sphere: tetrahedral cavity; NH<sub>2</sub> groups are omitted for clarity, due to disordered configuration

## Results and discussion

In this study, we deliberately chose water as the solvent because it is environmentally friendly, cheap, and suitable for scaled-up synthesis. Initially, we envisioned synthesizing the historically well-known UiO-66<sup>22</sup> from ZrOCl<sub>2</sub>·8H<sub>2</sub>O and terephthalic acid in water using acetic acid as a modulator. However, all our attempts failed irrespective of the experimental conditions because of the insolubility of terephthalic acid in water/acetic acid mixtures. We then turned our efforts to the synthesis of selected UiO-66-NH<sub>2</sub> from ZrOCl<sub>2</sub>·8H<sub>2</sub>O and H<sub>2</sub>BDC-NH<sub>2</sub>, on account of their appreciable solubility in water. Recently, some of us succeeded in synthesizing UiO-66-NH<sub>2</sub> from the disodium salt of 2-aminoterephthalate in ambient aqueous conditions using acetic acid modulator.<sup>23</sup> This study allowed us to demonstrate the need for the pre-treatment of zirconium cluster in the 50-70 °C temperature range, a condition requirement we assigned to the formation of the hexanuclear zirconium complexes, identified as the necessary building block for framework assembly. The reaction conditions selected were inspired from the literature.<sup>24,25</sup> To further enable the solubilization/dispersion of all reagents in water, H<sub>2</sub>BDC-NH<sub>2</sub> and saccharides were carefully ground prior synthesis. The subsequently increased particle surface resulted in a considerably better dissolution rate.<sup>26</sup> The grinding procedure took place using a laboratory-scale vibrating ball-mill for 10 min at 30 Hz. The ground reactants were then mixed with ZrOCl<sub>2</sub>·8H<sub>2</sub>O in a water/acetic acid mixture (10 mL/10 mL), and the solution was stirred at 90 °C for 24 h. After cooling down the solution at room temperature, the resulting solid materials were subjected to repeated centrifugation/washing steps using DMF, water and methanol consecutively.

To assess the influence of saccharides as co-modulators in the production of UiO-66-NH<sub>2</sub>, we first considered sorbitol in combination with acetic acid. Note that the amount of sorbitol was chosen for easy comparison with α-CD (which consists of 6 α-D-glucopyranoside units). After several consecutive cycles of centrifugation and washing, the powder was dried and analyzed by XRD (Figure 2). Poorly defined XRD patterns were observed corresponding to amorphous products, indicative of the poor performance of sorbitol as co-modulator for the growth of MOF crystallites.

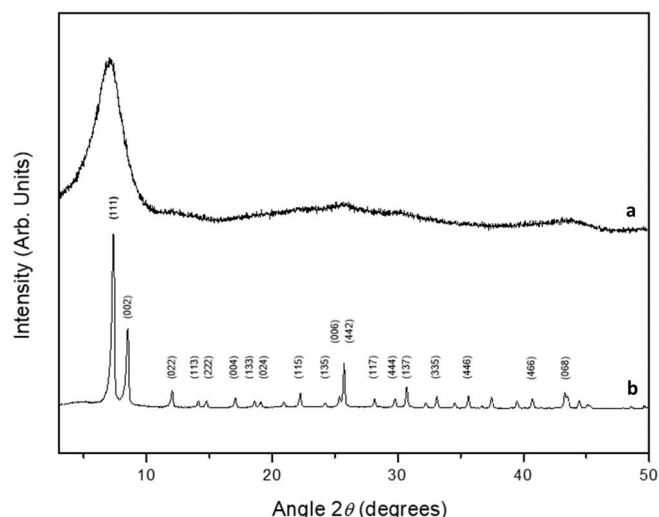


Fig 2. Powder XRD patterns of UiO-66-NH<sub>2</sub> derived from mixtures containing sorbitol (a) and α-D-methylglucopyranoside (b).

Notably, changing from sorbitol to α-D-methylglucopyranoside under the same experimental conditions resulted in the formation of UiO-66-NH<sub>2</sub> material of more crystalline nature as revealed by our XRD data (Figure 2). The powder pattern showed typical reflections of the face-centered-cubic structure of UiO-66-NH<sub>2</sub> with the *Fm-3m* space group (ESI, Figure S1).

α-CD was then used as a co-modulator under the same experimental conditions. Mixtures of acetic acid and α-CD gave similar XRD patterns, irrespective of the number of equivalents of α-CD with respect to the ligand, which is indicative of isostructural compounds (ESI, Figure S2). Indeed, no significant modification of the diffraction patterns was noticed upon increasing the proportion of α-CD up to 1 equivalent, suggesting that the lattice parameter and the crystallinity were not altered. We attribute the slight peak broadening observed at low modulator concentrations to the existence of nanocrystallites, according to previous reports.<sup>27</sup> The formation of UiO-66-NH<sub>2</sub> through the coordination interactions between Zr<sub>6</sub>-clusters and BDC-NH<sub>2</sub> ligands was further demonstrated through the alteration of several IR bands (ESI, Figures S3 and S4). The absorption bands were similar to those observed with α-D-methyl glucopyranoside except the bands assigned to acetic acid.<sup>22,28</sup> The absorption bands at 1496, 1382, 1336 cm<sup>-1</sup> were attributed to the stretching modes of the aromatic BDC-NH<sub>2</sub> bonds, and the bands at 1568 and 1423 cm<sup>-1</sup> were assigned to the stretching, asymmetric ( $\nu_{as}$ ) and symmetric ( $\nu_s$ ) vibrations of COO<sup>-</sup> groups, respectively (1257 cm<sup>-1</sup>  $\nu_{CO}$  simple).<sup>22,29</sup> Additional information about the UiO-66-NH<sub>2</sub> structures derived from α-CD as co-modulator was further extracted from the N<sub>2</sub> adsorption-desorption isotherms (Figure 3-A). For comparison, the isotherm of the control UiO-66-NH<sub>2</sub> prepared in the same conditions but without α-CD is also given. Overall, they display characteristic features of Type I adsorption isotherms, typical of microporous solids in which most pores have a size below 20 Å. The major gas consumption in the isotherms occurred at fairly low relative pressure ( $P/P^0 < 0.1$ ) before reaching a plateau. Table 1 lists the textural characteristics of the samples obtained with various amounts of the α-CD modulator, in terms of specific surface area (BET and Langmuir), micropore surface and volume, total volume and pore

size. With only acetic acid as modulator (no saccharide), the BET surface area was found to be  $611 \text{ m}^2\text{-g}^{-1}$  (Table 1, entry 1), which is in relative agreement with what was previously measured on hydrothermally prepared UiO-66-NH<sub>2</sub> samples in the literature ( $833 \text{ m}^2\text{-g}^{-1}$  and  $888 \text{ m}^2\text{-g}^{-1}$ ).<sup>14,23</sup> The slight discrepancy could be attributed

to the activation procedures, especially the preliminary grinding of H<sub>2</sub>BDC-NH<sub>2</sub>. Indeed, in our hands, the BET surface area was  $826 \text{ m}^2\text{-g}^{-1}$  when the linker was not ground.

Table 1. Textural characteristics of UiO-66-NH<sub>2</sub> synthesized in the presence of various amounts of  $\alpha$ -CD as co-modulator.

Entry	$\alpha$ -CD (equiv./ligand)	BET SSA ( $\text{m}^2/\text{g}$ ) <sup>a,b</sup>	Langmuir SSA ( $\text{m}^2/\text{g}$ ) <sup>c</sup>	$S_{\text{micro}}$ ( $\text{m}^2/\text{g}$ ) <sup>d</sup>	$S_{\text{micro}}/\text{BET SSA}$ (%)	$V_{\text{micro}}$ ( $\text{cm}^3/\text{g}$ ) <sup>e</sup>	$V_{\text{total}}$ ( $\text{cm}^3/\text{g}$ ) <sup>f</sup>	$V_{\text{micro}}/V_{\text{total}}$ (%)	Average pore diameter ( $\text{\AA}$ ) <sup>g</sup>
1	0	$611 \pm 6$	$706 \pm 11$	424	69.5	0.144	0.268	54.1	17.7
2	0.05	$854 \pm 5$	$1024 \pm 6$	546	63.5	0.184	0.408	45.0	19.1
3	0.10	$924 \pm 6$	$1071 \pm 9$	631	68.3	0.216	0.410	52.6	17.8
4	0.25	$1071 \pm 15$	$1182 \pm 9$	775	72.6	0.268	0.429	62.4	16.1
5	0.50	$1136 \pm 17$	$1232 \pm 14$	847	74.6	0.293	0.443	66.4	15.6
6	0.75	$1198 \pm 18$	$1292 \pm 13$	891	74.7	0.310	0.462	67.0	15.5
7	1	$1451 \pm 4$	$1589 \pm 5$	1085	74.7	0.373	0.575	64.9	15.9
8	1.25	$878 \pm 4$	$1069 \pm 6$	623	71.0	0.215	0.454	47.5	20.7
9	1.50	$80 \pm 1$	$107 \pm 1$	47	58.5	0.016	0.059	26.7	26.7
10	2	$45 \pm 2$	$62 \pm 3$	22	49.5	0.006	0.037	16.2	33.0
11 <sup>h</sup>	1	$772 \pm 17$	$866 \pm 35$	535	69.3	0.183	0.317	57.8	16.5

<sup>a</sup> Average of at least two experiments. <sup>b</sup> Specific surface area calculated from the Brunauer-Emmett-Teller equation in the  $P/P^\circ$  range from 0.001 to 0.05; <sup>c</sup> Specific surface area calculated from the Langmuir equation in the  $P/P^\circ$  range from 0.001 to 0.70; <sup>d</sup> Micropore surface area determined by the t-plot method; <sup>e</sup> Micropore volume determined by the t-plot method; <sup>f</sup> Total pore volume estimated at  $P/P^\circ = 0.95$ ; <sup>g</sup> Average pore size based on  $4 \times V_{\text{total}}/\text{BET SSA}$ ; <sup>h</sup> Prepared without grinding  $\alpha$ -CD and H<sub>2</sub>BDC-NH<sub>2</sub> ligand.

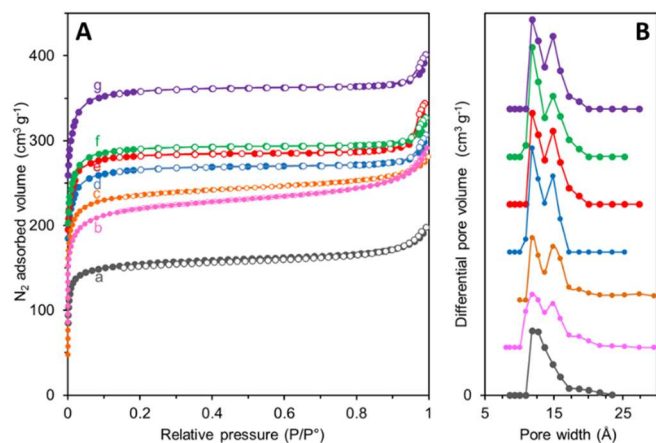


Fig 3. (A) N<sub>2</sub> sorption isotherms collected at 77 K of NH<sub>2</sub>-UiO-66 synthesized using various amounts of ground  $\alpha$ -CD with respect to ground H<sub>2</sub>BDC-NH<sub>2</sub> [Adsorption (filled circles) and desorption (open circles)]. (B) with the corresponding pore size distribution plots determined via NLDFT: 0 equiv.  $\alpha$ -CD/ H<sub>2</sub>BDC-NH<sub>2</sub> (a, grey), 0.05 equiv. (b, pink), 0.10 equiv. (c, orange), 0.25 equiv. (d, blue), 0.5 equiv. (e, red), 0.75 equiv. (f, green), and 1 equiv. (g, violet).

Note that all BET surface areas were calculated using the consistency criteria recommended by Rouquerol *et al.*<sup>30</sup> for selecting the appropriate linear pressure range (i.e. 0.001 – 0.05). A proportion of

micropore ( $V_{\text{micro}}/V_{\text{total}}$ ) of ca. 54 % was found, this value being very consistent with the observation of Zhou *et al.* (55.9 %).<sup>31</sup>

We then investigated the influence of the amount of  $\alpha$ -CD on the textural properties of UiO-66-NH<sub>2</sub>. Notably, the porosity was greatly enhanced when the Zr-MOFs were produced in the presence of acetic acid/ $\alpha$ -CD mixtures. For instance, using an  $\alpha$ -CD/linker molar ratio of as low as 0.25, the BET specific surface area increased from 611 to 1071  $\text{m}^2\text{-g}^{-1}$  and the total pore volume from 0.268 to 0.429  $\text{cm}^3\text{-g}^{-1}$  (Table 1, entries 2-4). The micropore surface area and micropore volume were also enhanced by the use of  $\alpha$ -CD, by an extent ranging from 424 to 775  $\text{m}^2\text{-g}^{-1}$  and from 0.144 to 0.268  $\text{cm}^3\text{-g}^{-1}$  respectively. The microporous structure can be verified by the pore size distribution (PSD) derived from nonlocal density functional theory (NLDFT). The PSD was altered in the micropore region, showing a bimodal distribution with pores diameters centered at about 11.8  $\text{\AA}$  and 14.8  $\text{\AA}$  (Figure 3-B), in good agreement with the literature.<sup>32,33</sup> The porosity of the UiO-66-NH<sub>2</sub> samples was further enhanced upon the addition of higher quantities of  $\alpha$ -CD, as illustrated in Figure 4 through their BET and Langmuir specific surface areas. UiO-66-NH<sub>2</sub> prepared with 1 equivalent of  $\alpha$ -CD with respect to the H<sub>2</sub>BDC-NH<sub>2</sub> ligand featured a BET specific surface area of 1451  $\text{m}^2\text{-g}^{-1}$ , a Langmuir surface of 1589  $\text{m}^2\text{-g}^{-1}$  (Table 1, entry 7).

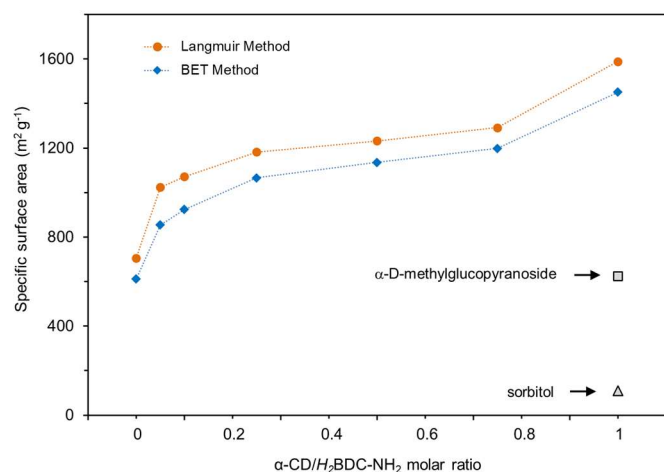


Fig 4. Variation of the specific surface area (SSA) of UiO-66-NH<sub>2</sub> with the amount of  $\alpha$ -CD. SSA calculated for UiO-66-NH<sub>2</sub> synthesized using sorbitol or  $\alpha$ -D-methylglucopyranoside as saccharide sources were added for comparison. ● calculated using the Langmuir method, ◆ calculated using the BET method.

As usually observed, slightly higher Langmuir surface areas were obtained for all the hereby synthesized UiO-66-NH<sub>2</sub>, irrespective of the  $\alpha$ -CD/ligand ratio. Indeed, it is commonly accepted that the Langmuir theory (based on monolayer adsorption) tends to overestimate the apparent surface area of the MOFs.<sup>34</sup> While the PSD was not significantly altered, being centered at ca. 11.8 and 14.8 Å, calculation of the proportion of micropore volume once again revealed that high degrees of microporosity were maintained, reaching approximately 65%. This result is consistent with the increased dangling (or pending) linkers<sup>24</sup> percentage within the framework, possibly due to competitive equilibria.<sup>35,36</sup> Interestingly, this trend obtained with N<sub>2</sub> adsorption measurements was also observed using CO<sub>2</sub> as adsorbate (adsorption at 273 K), in line with the overall increase in microporosity in UiO-66-NH<sub>2</sub> materials prepared from  $\alpha$ -CD (ESI, Figure S5). Astonishingly, we observed that the addition over 1 equivalent of  $\alpha$ -CD with respect to the linker, resulted in a dramatic decrease in the specific surface area from 1451 m<sup>2</sup>·g<sup>-1</sup> to 51 m<sup>2</sup>·g<sup>-1</sup> (Table 1, entries 8-10; ESI, Figure S6). Overall, our results indicate that the stoichiometric  $\alpha$ -CD / linker molar ratio appears to be the upper limit of the beneficial effect of  $\alpha$ -CD as co-modulator. Table 1 also revealed the advantage of ground materials over unground materials. Indeed, comparing Entries 7 and 11 clearly showed that the unground material led to lower SSA. Unground CDs are probably less dispersed and less available to play their role of co-modulator. Accordingly, grinding  $\alpha$ -CD and linkers has a beneficial influence on its dispersion in the aqueous solution. Indeed, the MOF synthesis took place in an aqueous dynamic heterogeneous medium wherein the components were not fully soluble. It is also worth noting that, when the synthesis was performed with sorbitol using a 1/1 saccharide / linker molar ratio, the BET SSA value was dramatically reduced to 110 m<sup>2</sup>·g<sup>-1</sup>. With  $\alpha$ -D-methylglucopyranose as constitutive building blocks for CD, the BET SSA value was 625 m<sup>2</sup>·g<sup>-1</sup>, a value similar to that obtained with the control (no saccharide, SSA = 611 m<sup>2</sup>·g<sup>-1</sup>). This is in stark contrast with our results on  $\alpha$ -CD.

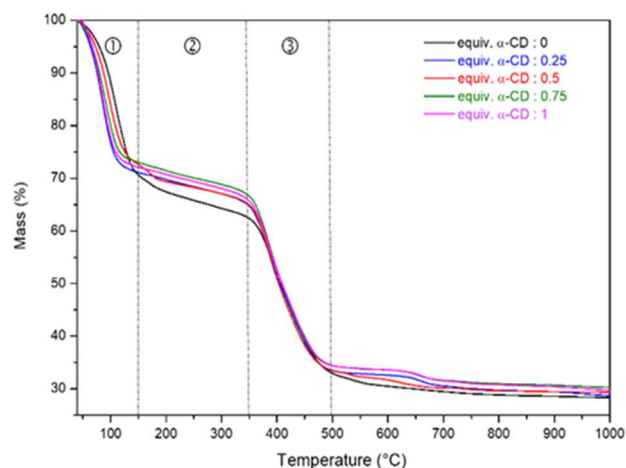


Fig 5. TGA curves of UiO-66-NH<sub>2</sub> synthesized under modulated hydrothermal conditions using  $\alpha$ -CD to ligand ratios of 0 (black), 0.25 (blue), 0.5 (red), 0.75 (green), and 1 (purple).

Thermogravimetric analysis (TGA, Figure 5) was also carried out to evaluate the thermal stability of the UiO-66-NH<sub>2</sub> derived from  $\alpha$ -CD.<sup>28,37</sup> The resulting TGA profiles revealed three primary stages of mass loss. After dehydration of the MOF structure from 100 to 150 °C, we observed the dehydroxylation of the Zr<sub>6</sub>-nodes between 150 and 350 °C. In this temperature range, the  $\mu^3$ -OH coordinated hydroxyl groups were partly removed, resulting in the transformation of the SBU from [Zr<sub>6</sub>O<sub>4</sub>(OH)<sub>4</sub>]<sup>12+</sup> to [Zr<sub>6</sub>O<sub>6</sub>]<sup>12+</sup>.<sup>38</sup> The third thermal event, observed from 350 to 500 °C, corresponds to the exothermic decomposition of the linker. This temperature range at which decomposition occurred, was lower than that reported, usually around 500-550 °C for MOFs synthesized under solvothermal conditions (ZrCl<sub>4</sub> in DMF).<sup>39,40</sup> Over 500 °C, we observed the decomposition of the framework with only ZrO<sub>2</sub> as the final residue, as confirmed by additional XRD (ESI, Figure S7) and DSC analyses (ESI, Figure S8). Throughout the heating process, TG curves relative to MOFs synthesized from various  $\alpha$ -CD/linker ratios clearly show that the thermal stability does not significantly depend on the amount of  $\alpha$ -CD. Indeed, all the TG curves are superimposable. This is in line with the hypothesis that CDs do not create defects within the bulk MOF structure. Additionally, no significant difference was observed in the FTIR spectra regardless the amount of  $\alpha$ -CD (ESI, Figure S4). Noteworthy, our results did not show any characteristic vibration bands for  $\alpha$ -CD, which indicates that the latter is not contributing to the MOF structure and is removed during the washing process.

To unequivocally exclude the presence of  $\alpha$ -CD within the MOF structure or on the peripheral surface of UiO-66-NH<sub>2</sub> crystallites, we also performed digestion experiments of UiO-66-NH<sub>2</sub> (see the protocol in the ESI). We first undertook aqueous alkaline digestion experiments of UiO-66-NH<sub>2</sub> using NaOH. The <sup>1</sup>H NMR spectrum of the degraded UiO-66-NH<sub>2</sub> only showed signals corresponding to the aromatic protons of the linker (ESI, Figure S9). No trace of  $\alpha$ -CD was detected, strongly indicating the complete absence of  $\alpha$ -CD. Accordingly, the role of  $\alpha$ -CD can therefore be rationalized as a true co-modulator, facilitating the crystallization process without being incorporated into the metal-organic framework.

In order to assess the defect concentration in the UiO-66-NH<sub>2</sub> samples synthesized with the use of  $\alpha$ -CD co-modulator, the modulator to linker ratio needs to be quantified. To determine the

number of acetic acid and  $H_2BDC-NH_2$  molecules per Zr node, an acidic digestion<sup>41</sup> of the MOF was carried out in the presence of maleic acid as an internal reference.<sup>42</sup> From the relative peak area of the distinctive aromatic BDC- $NH_2$  protons (d 7.12 ppm ; s 7.46 ppm ; d 7.79 ppm) and acetic acid methyl protons (2.52 ppm), the amount of modulator was found to be quite constant for the various samples, in the range from 0.08 to 0.11 per  $\{Zr_6\}$ -cluster, whereas the amount of BDC- $NH_2$  linker was found to vary more significantly from 5.95 down to 5.08 per  $\{Zr_6\}$ -cluster (ESI, Table S1). It should be noted that in the ideal non-defected structure, there would be 6 BDC and 0 acetate per inorganic nodes. Hence, we can conclude that the synthesized MOFs show very few defects within their structures, irrespective of the amount of  $\alpha$ -CD. The MOF structure obtained using 1 equiv.  $\alpha$ -CD with respect to the linker can be formulated as  $Zr_6O_4(OH)_{4.85}(BDC-NH_2)_{5.52}(CH_3COO)_{0.11}$ , indicative of 0.85 out of 12 linkers missing per  $\{Zr_6\}$ -cluster.

When using  $\beta$ -CD (which consists of 7  $\alpha$ -D-glucopyranoside units) as co-modulator instead of  $\alpha$ -CD, under the same experimental conditions, no modification of the XRD patterns (ESI, Figure S10) and FTIR spectra (ESI, Figure S11 and S12) was noticed. Once again, this demonstrates the integrity of the UiO-66- $NH_2$  structure.

All the  $N_2$  adsorption-desorption isotherms obtained with this series prepared with  $\beta$ -CD can be still classified as type I, typical of microporous samples (ESI, Figure S13). Furthermore, we observed a strong dependence of the amount and proportion of the co-modulator  $\beta$ -CD on the samples' textural properties. Our results evidenced that we were able to optimize porosity by adjusting the  $\beta$ -CD/linker ratio to 0.5 (Figure 6), which, in these conditions, is similar to that measured with  $\alpha$ -CD (ESI, Figure S6). The total pore volume was  $0.458\text{ cm}^3\cdot\text{g}^{-1}$ . The BET and Langmuir surface areas of near defect free UiO-66- $NH_2$  were 1187 and 1287  $\text{m}^2\cdot\text{g}^{-1}$ , respectively (ESI, Table S2). Interestingly such values are similar to those obtained using organic solvents, thus revealing the effect of CDs on the SSA of near defect free UiO-66- $NH_2$ . It is also worth remembering that, in the literature, the highest value reported so far for the SSA of UiO-66- $NH_2$  synthesized under aqueous conditions in a batch reactor was only 888  $\text{m}^2\cdot\text{g}^{-1}$ . Above this  $\beta$ -CD/linker ratio of 0.5, some degree of porosity was sacrificed, but typical specific surface areas could be retained even for the sample obtained using 1 equiv. of CD (displaying reduced BET and Langmuir SSA values of 801 and 889  $\text{m}^2\cdot\text{g}^{-1}$ , respectively). This demonstrates that  $N_2$  uptake and specific surface areas may be optimized by the judicious control of  $\beta$ -CD/linker ratios.

In order to get further insight into the role of CDs in aqueous synthesis of UiOs, and to assess their performance as a function of their size,  $\gamma$ -CD (which consists of 8  $\alpha$ -D-glucopyranoside units) was also used as a modulator in the synthesis of UiO-66- $NH_2$ . Surprisingly, we observed that the modulator's effect on the textural properties of UiO-66- $NH_2$  was deleterious (ESI, Figure S14), although the XRD patterns (ESI, Figure S15) and FTIR spectra (ESI, Figures S16 and S17) revealed that the UiO topology was maintained. Increasing the proportion of  $\gamma$ -CD from 0 to 1 equivalent of  $\gamma$ -CD with respect to the linker provoked a dramatic decrease in the surface area from 611 to 39  $\text{m}^2\cdot\text{g}^{-1}$  for the BET model and from 706 to 59  $\text{m}^2\cdot\text{g}^{-1}$  for the Langmuir model (Figure 7). This trend seems to be indicative of the destabilization effect of  $\gamma$ -CD on the crystal growing MOF, thereby creating defects and limiting the MOF crystal size. This was further proved by the subsequent  $N_2$  uptake.  $N_2$  uptake was only  $0.035\text{ cm}^3\cdot\text{g}^{-1}$  for UiO-66- $NH_2$  synthesized using 1 equivalent of  $\gamma$ -CD with respect to the linker (ESI, Table S3).

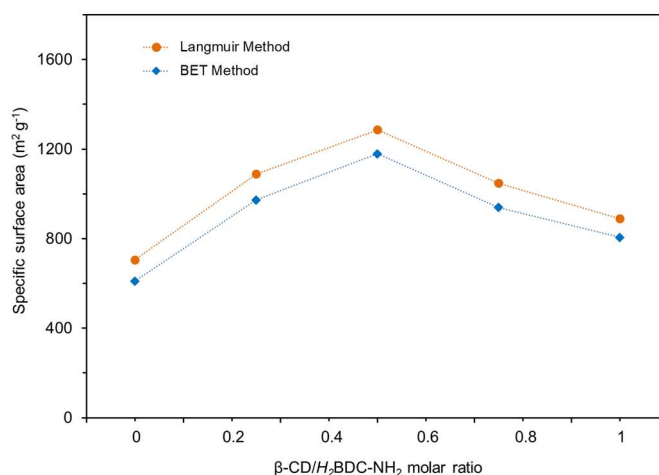


Fig 6. Variation of the specific surface area of UiO-66- $NH_2$  as a function of the amount of  $\beta$ -CD. ■ calculated using the Langmuir method, ◆ calculated using the BET method.

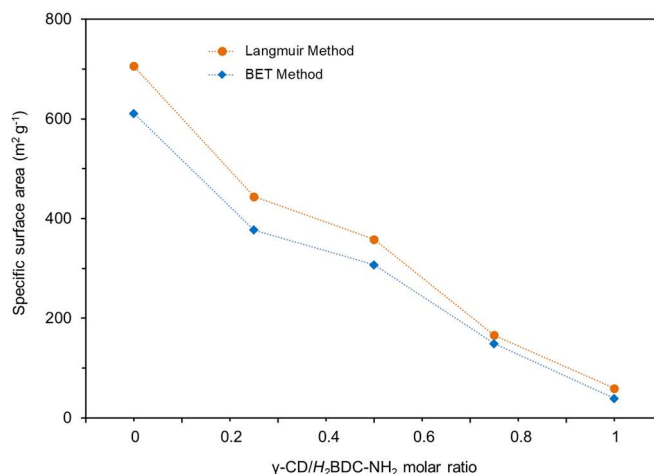


Fig 7. Variation of the specific surface area of UiO-66- $NH_2$  as a function of the amount of  $\gamma$ -CD. ■ calculated using the Langmuir method, ◆ calculated using the BET method.

Field emission scanning electron microscopy (FE-SEM) was used to investigate the crystallite morphology. Figure 8 depicts typical FE-SEM images of three selected UiO-66- $NH_2$  samples prepared without cyclodextrin (control) and, with 0.5 equiv. of  $\alpha$ -CD or 0.5 equiv. of  $\beta$ -CD at magnifications of 25,000 and 50,000. Notably, the particle morphology was found to be similar without or with cyclodextrin as co-modulators. Overall, the SEM pictures showed that the materials are comprised of densely packed particles whose shapes mostly polygonal with straight or gently curved grain boundaries. Nevertheless, it can be noticed that the average size of the polygonal particles slightly differs depending on the sample. Therefore, compared to the control UiO sample (without cyclodextrin), which produce small monodisperse particles typically ranging from 100 to 200 nm in size (Figure 8-a and Figure 8-b), slightly more polydisperse and larger crystallites were observed for UiO-66- $NH_2$  synthesized with  $\alpha$ -CD (Figure 8-c and Figure 8-d) and  $\beta$ -CD (Figure 8-e and Figure 8-f) as co-modulators.

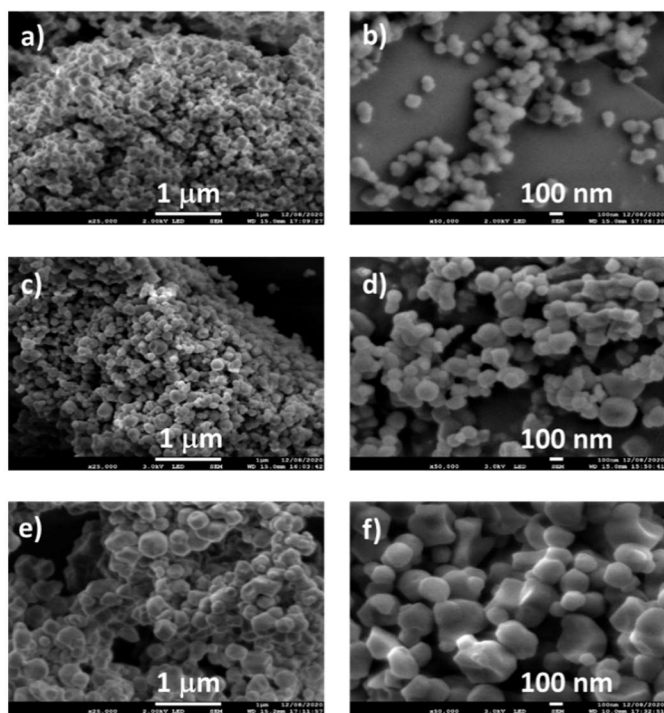


Fig 8. Representative FE-SEM images of UiO-66-NH<sub>2</sub> synthesized without  $\alpha$ -CD (a and b), with 0.5 equiv.  $\alpha$ -CD with respect to the linker (c and d), and with 0.5 molar equiv. of  $\beta$ -CD with respect to the linker (e and f). Magnification: 25,000x (left column) and 50,000x (right column).

Especially in the latter case, the impact on the grain dimension seems to be even more pronounced, with sizes that could sometimes reach or exceed 450 nm (ESI, Figure S18).

Complementary experiments were carried out to better understand the role of CDs. Photographs of aqueous solutions containing the Zr precursor and the linker were compared at various mixing time if CDs was added or not as a co-modulator. They clearly showed a bad dispersion of the materials without CD (especially at the beginning of the synthesis), and a good dispersion of the reactants in the presence of CDs (ESI, Figure S19). We also investigated the interaction of the preformed Zr<sub>6</sub>O<sub>4</sub>(OH)<sub>4</sub>(CH<sub>3</sub>COO)<sub>12</sub> oxyacetate cluster with CDs by NMR. To this end, 2D T-ROESY NMR measurements were performed to determine the inclusion ability of the three CDs towards H<sub>2</sub>BDC-NH<sub>2</sub> and Zr<sub>6</sub>-clusters in water. While no cross-peak was detected in the 2D T-ROESY NMR spectrum of a stoichiometric mixture of  $\alpha$ -CD/H<sub>2</sub>BDC-NH<sub>2</sub> and  $\alpha$ -CD/Zr<sub>6</sub>-clusters in D<sub>2</sub>O at 25 °C (ESI, Figure S20 and S21), strong correlations were revealed in the spectrum of  $\beta$ -CD/H<sub>2</sub>BDC-NH<sub>2</sub><sup>43</sup> (ESI, Figure S22), indicative of the inclusion of H<sub>2</sub>BDC-NH<sub>2</sub> into  $\beta$ -CD.  $\beta$ -CD is well-known to interact with aromatic compounds to form inclusion complexes.<sup>44</sup> However, no correlation was detected for a  $\beta$ -CD/Zr<sub>6</sub>-clusters stoichiometric mixture (ESI, Figure S23), indicating that the Zr<sub>6</sub>-node was not included into the  $\beta$ -CD cavity. As expected, no correlation was observed on the 2D T-ROESY NMR spectrum of  $\gamma$ -CD/H<sub>2</sub>BDC-NH<sub>2</sub> either (ESI, Figure S24), the molecular recognition of  $\gamma$ -CD towards H<sub>2</sub>BDC-NH<sub>2</sub> is poor because the  $\gamma$ -CD cavity is too wide. Note that no interaction was observed between  $\gamma$ -CD with the cluster (ESI, Figure 25).

Based on all the above results, we sought to develop a mechanistic insight into the roles of CDs on the MOF growth. As initially envisaged,  $\alpha$ -CD,  $\beta$ -CD and  $\gamma$ -CD could interact differently with the Zr<sub>6</sub>-clusters as co-modulators, while other saccharides did not. This strongly suggests that the CD structure plays an important role in modulating the dynamic motion of the frameworks. It is known that the complexation of native CDs with metal ions can affect the supramolecular arrangements and packing, as recently reviewed.<sup>45,46</sup> Besides the connection with the carboxylate groups of acetic acid, the growing peripheral sites of UiO-66-NH<sub>2</sub> could be temporarily stabilized by CDs that greatly alter the growing process to generate highly ordered structures. We suggest that, during the MOF crystal growth process,  $\alpha$ -CD,  $\beta$ -CD and  $\gamma$ -CD regulate the coordination of BDC-NH<sub>2</sub> ligands onto the Zr<sub>6</sub>-clusters to form regular MOF structures (Figure 9). From the dimensions of CDs and Zr-clusters, three cases could be distinguished.  $\gamma$ -CD (external diameter = 1.75 nm; internal diameter = 0.75-0.83 nm)<sup>47</sup> hampers the coordination of BDC-NH<sub>2</sub> to the Zr<sub>6</sub>-cluster ( $\phi \sim 1.1$  nm), resulting in a poorly-defined MOF structure.<sup>48</sup> Indeed,  $\gamma$ -CD could transiently include the Zr<sub>6</sub> clusters in line with the respective sizes. This hypothesis agrees with data from the literature. Indeed, it is reported that  $\gamma$ -CD could spontaneously interact with a number of different oxo- and metal-clusters that can be described as nanoscale objects of about typically 2.5-3 nm in diameter.<sup>49-50,51,52</sup> Conversely, the smaller size of  $\alpha$ -CD (external diameter = 1.46 nm; internal diameter = 0.47 - 0.53 nm)<sup>47</sup> would not disturb the BDC-NH<sub>2</sub> bonding formation with the Zr<sub>6</sub>-clusters to make the 3D infinite framework. The respective dimensions of  $\alpha$ -CD and Zr<sub>6</sub>-clusters would not permit inclusion of the cluster within the  $\alpha$ -CD cavity.  $\beta$ -CD, for its part, has an intermediate behavior between  $\alpha$ -CD and  $\gamma$ -CD because of its dimensions (external diameter = 1.54 nm; internal diameter = 0.60 – 0.65 nm)<sup>47</sup>.  $\beta$ -CD being wider than  $\alpha$ -CD, its interaction area with Zr<sub>6</sub>-clusters could be greater. Therefore, a smaller amount of the  $\beta$ -CD may already lead to MOF growth inhibition. However, in a well-defined concentration range, the effect of  $\beta$ -CD on the MOF structure is determining as the largest crystallites obtained in this study result from the utilization of  $\beta$ -CD as co-modulator (Figure 8). Our results could also be rationalized by other concomitant phenomena. Firstly, CDs could act as dispersing agents. As evidenced by photographs on the suspension of the reactants (ESI, Figure S19),  $\alpha$ -CD facilitates the dispersion of H<sub>2</sub>BDC-NH<sub>2</sub> (which is not fully solubilized in water) via adsorption on hydrophobic linker aggregates. Indeed, the possibility could not be excluded that  $\alpha$ -CD interacts with linker aggregates. In the literature, it has already been shown that CDs help dispersing hydrophobic organic particles in aqueous media.<sup>53,54</sup> In our case, the improved dispersion enables the growth of UiO-66-NH<sub>2</sub> featuring record high SSA reported so far for aqueous syntheses. Secondly, CDs could form supramolecular inclusion complexes with the linker. As revealed by 2D NMR experiments,  $\beta$ -CD also probably participates in the inclusion of H<sub>2</sub>BDC-NH<sub>2</sub> within its cavity, while  $\alpha$ -CD and  $\gamma$ -CD are unable to do so. The formation of such supramolecular interaction is clearly not favorable to the MOF growth. Hence, when the concentration of  $\beta$ -CD is too high, such inclusion complex between  $\beta$ -CD and the linker may displace equilibria to such an extent that the amount of non-included linker became sub-stoichiometric with respect to Zr<sub>6</sub>-clusters, resulting in MOF structures featuring lower SSA.

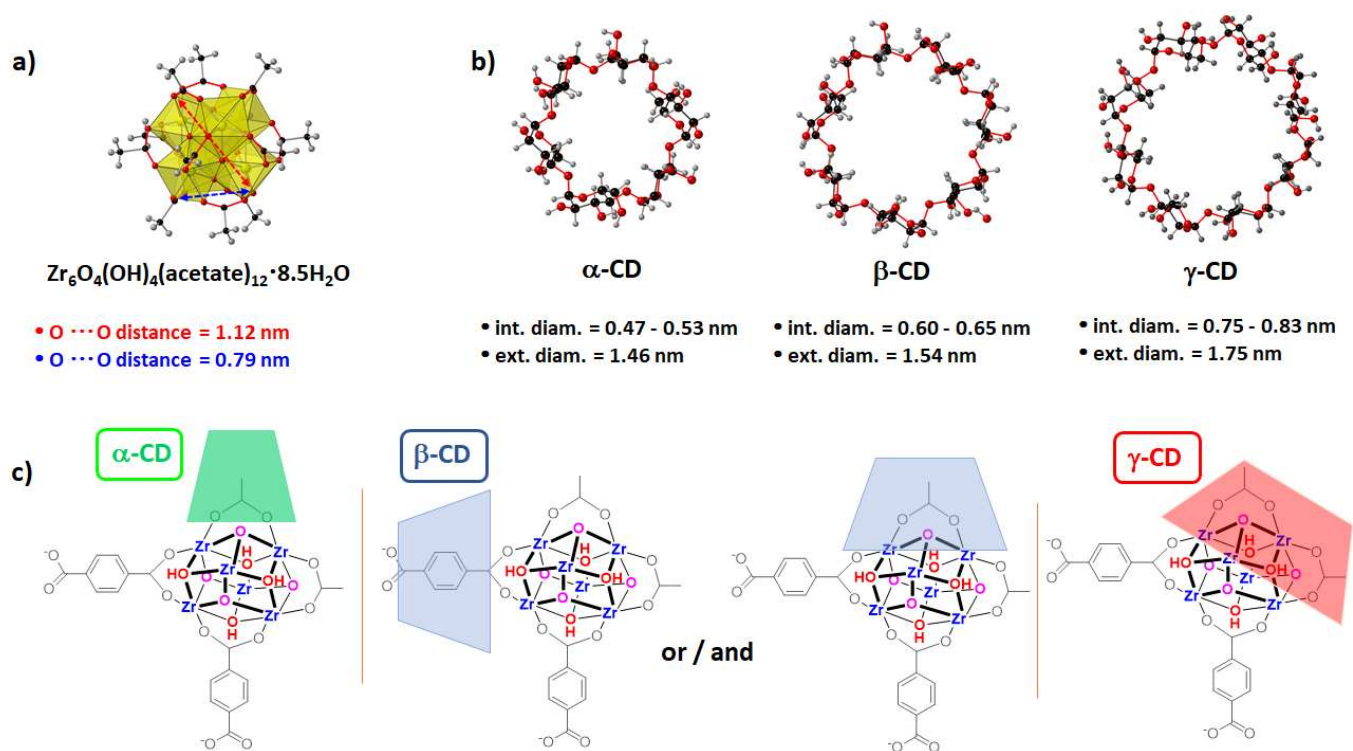


Fig 9. a) Structural representation of a molecular oxo-acetato  $\{\text{Zr}_6\}$ -cluster highlighting the longest (1.12 nm) and shortest (0.79 nm) intracluster O...O distances, as defined by the red and blue arrows. From reference 48. b) Structural representations of native cyclodextrins ( $\alpha\text{-CD}$ ,  $\beta\text{-CD}$  and  $\gamma\text{-CD}$ ) with their average internal and external diameters. From reference 47. c) Possible interactions of  $\alpha\text{-CD}$ ,  $\beta\text{-CD}$  and  $\gamma\text{-CD}$  with the  $\{\text{Zr}_6\}$ -cluster. Color scheme: Zr white, O red, C black, H grey.

## Experimental

### Modulated hydrothermal synthesis of UiO-66-NH<sub>2</sub>

ZrOCl<sub>2</sub>·8H<sub>2</sub>O (0.322 g, 1 mmol) was dissolved in a mixture of water/acetic acid (5 mL/5 mL). 2-aminoterephthalic acid (0.181 g, 1 mmol) and the saccharide were ground under ball-milling conditions (15 min, 30 Hz) and then added to the preformed Zr acetate precursor in the previous solution. The reaction mixture was heated at 90 °C for 24 h. The precipitate was then washed successively with DMF (2 × 10 mL), water (2 × 10 mL) and methanol (2 × 10 mL) to remove residual reagents from the MOF pores. The sample was dried under vacuum at 100 °C for 24 h to yield the final product.

## Conclusions

In conclusion, we have developed a new procedure to promote the synthesis of UiO-66-NH<sub>2</sub> under aqueous conditions. Our strategy relies on the use of both acetic acid and saccharides as co-modulators. By simply introducing appropriate saccharides as co-modulators in well-defined quantity, we can control the growth of UiO-66-NH<sub>2</sub> featuring high SSA and N<sub>2</sub> sorption properties. While sorbitol leads to amorphous structures, the utilization of  $\alpha\text{-D}$ -methylglucopyranoside as co-modulator has no effect on the SSA and N<sub>2</sub> sorption properties.  $\gamma\text{-CD}$ , for its part, proves to be inappropriate as it prevents the growth of Zr-

MOF. Conversely,  $\alpha\text{-CD}$  and  $\beta\text{-CD}$  in well-defined concentration ranges act as very effective co-modulators in combination with acetic acid. While CD-free aqueous syntheses of Zr-MOFs typically result in altered properties when compared to solvothermal approaches, hydrothermal syntheses of Zr-MOFs in the presence of  $\alpha\text{-CD}$  and  $\beta\text{-CD}$  were found to reproduce them. Through modulated synthesis,  $\alpha\text{-CD}$  and  $\beta\text{-CD}$  bind competitively to the metal clusters during framework formation, resulting in crystalline products with higher porosity and SSA compared to Zr-MOFs obtained under typical aqueous conditions. Additionally, CDs help dispersing the poorly water-soluble H<sub>2</sub>BDC-NH<sub>2</sub> linker and facilitate its coordination to Zr clusters. Investigations are currently on-going to widen the scope of the strategy herein developed to other MOFs.

## Conflicts of interest

There are no conflicts to declare.

## Acknowledgements

The authors acknowledge the Chevreul Institute (FR 2638), Ministère de l'Enseignement Supérieur et de la Recherche, Région Hauts de France and FEDER program for supporting and partially funding this work. Guillaume Hoyez is grateful to the University of Artois for the funding of his PhD grant. We thank

also Dr. Ahmed Addad (UMET, University of Lille) and Prof. Christian Mathieu (UCCS, University of Artois) for FE-SEM analyses, Dr. Jérémy Ternel (UCCS, University of Artois) for NMR analyses and Dr. Nicolas Kania (UCCS, University of Artois) for TGA measurements.

## Notes and references

---

- <sup>1</sup> M. Li, D. Li, M. O'Keeffe, and O.M. Yaghi, *Chem. Rev.*, 2013, **114**, 1343–1370.
- <sup>2</sup> S. Yuan, L. Feng, K. Wang, J. Pang, M. Bosch, C. Lollar, Y. Sun, J. Qin, X. Yang, P. Zhang, Q. Wang, L. Zou, Y. Zhang, L. Zhang, Y. Fang, J. Li and H.-C Zhou, *Adv. Mat.*, 2018, 1704303.
- <sup>3</sup> L. T. L. Nguyen, K. K. A. Le, H. X. Truong and N. T. S. Phan, *Catal. Sci. Technol.*, 2012, **2**, 521–528.
- <sup>4</sup> S. Marx, W. Kleist and A. Baiker, *J. Catal.*, 2011, **281**, 76–87.
- <sup>5</sup> K. Leus, M. Vandichel, Y.-Y. Liu, I. Muylaert, J. Musschoot, S. Pyl, H. Vrielinck, F. Callens, G. B. Marin, C. Detavernier, P. V. Viper, Y. Z. Khimiyak, M. Waroquier, V. Van Speybroeck and P. Van der Voort, *J. Catal.*, 2012, **285**, 196–207.
- <sup>6</sup> O. Kozachuk, I. Luz, F. X. Llabrés i Xamena, H. Noei, M. Kauer, H. B. Albada, E. D. Bloch, B. Marler, Y. Wang, M. Muhler and R. A. Fischer, *Angew. Chem. Int. Ed.*, 2014, **53**, 7058–7062.
- <sup>7</sup> J.-Y. Ye and C.-J. Liu, *Chem. Commun.*, 2011, **47**, 2167–2169.
- <sup>8</sup> Y. Liu, R. C. Klet, T. Hupp and O. Farha, *Chem. Commun.*, 2016, **52**, 7806–7809.
- <sup>9</sup> W. Zhang, M. Kauer, O. Halbherr, K. Epp, P. Guo, M. I. Gonzalez, D. J. Xiao, C. Wiktor, F. X. Llabrés i Xamena, C. Wöll, Y. Wang, M. Muhler and R. A. Fischer, *Chem. Eur. J.*, 2016, **22**, 14297–14307.
- <sup>10</sup> F. C. Cirujano, A. Corma and F. X. Llabrés i Xamena, *Chem. Eng. Sci.*, 2015, **124**, 52–60.
- <sup>11</sup> S. Dissegna, R. Hardian, K. Epp, G. Kieslich, M.-V. Coulet, P. Llewellyn and R. A. Fischer, *CrystEngComm*, 2017, **19**, 4137–4141.
- <sup>12</sup> A. Schaate, P. Roy, A. Godt, J. Lippke, F. Waltz, M. Wiebcke and P. Behrens, *Chem. Eur. J.*, 2011, **17**, 6643–6651.
- <sup>13</sup> Z. Hu, I. Castano, S. Wang, Y. Wang, Y. Peng, Y. Qian, C. Chi, X. Wang, and D. Zhao, *Cryst. Growth Des.*, 2016, **16**, 2295–2301.
- <sup>14</sup> Z. Hu, Y. Peng, Z. Kang, Y. Qian and D. Zhao, *Inorg. Chem.*, 2015, **54**, 4862–4868.
- <sup>15</sup> M. J. Van Vleet, T. Weng, X. Li and J. R. Schmidt, *Chem. Rev.*, 2018, **118**, 3681–3721.
- <sup>16</sup> G. C. Shearer, S. Chavan, S. Bordiga, S. Svelle, U. Olsbye and K. P. Lillerud, *Chem. Mater.*, 2016, **28**, 3749–3761.
- <sup>17</sup> A. Schaate, P. Roy, T. Preuße, S. J. Lohmeier, A. Godt and P. Behrens, *Chemistry*, 2011, **17**, 9320–9325.
- <sup>18</sup> F. Vermoortele, B. Bueken, G. Le Bars, B. Van de Voorde, M. Vandichel, K. Houthoofd, A. Vimont, M. Daturi, M. Waroquier, V. Van Speybroeck, C. Kirschhock and D. E. De Vos, *J. Am. Chem. Soc.*, 2013, **135**, 11465–11468.
- <sup>19</sup> M. J. Cliffe, W. Wan, X. Zou, P. A. Chater, A. K. Kleppe, M. G. Tucker, H. Wilhelm, N. P. Funnell, F.-X. Coudert and A. L. Goodwin, *Nat. Commun.*, 2014, **5**, 4176.
- <sup>20</sup> S. J. Garibay and S. M. Cohen, *Chem. Commun.*, 2010, **46**, 7700–7702.
- <sup>21</sup> M. Kandiah, M. Hellner Nilsen, S. Usseglio, S. Jakobsen, U. Olsbye, M. Tilset, C. Larabi, E. A. Quadrelli, F. Bonino and K. P. Lillerud, *Chem. Mater.*, 2010, **22**, 6632–6640.
- <sup>22</sup> J. Hafizovic Cavka, S. Jakobsen, U. Olsbye, N. Guillou, C. Lamberti, S. Bordiga and K. P. Lillerud, *J. Am. Chem. Soc.*, 2008, **130**, 13850–13851.
- <sup>23</sup> I. Pakamoré, J. Rousseau, C. Rousseau, E. Monflier and P. Ágota Szilágyi, *Green Chem.*, 2018, **20**, 5292–5298.
- <sup>24</sup> Z. Hu, Y. Peng, Z. Kang, Y. Qian and D. Zhao, *Inorg. Chem.*, 2015, **54**, 4862–4868.
- <sup>25</sup> H. Reinsch, S. Waitschat, S. M. Chavan, K. P. Lillerud and N. Stock, *Eur. J. Inorg. Chem.*, 2016, 4490–4498.
- <sup>26</sup> M. Nakach, J.-R. Authelin, A. Chamayou and J. Dodds, *Int. J. Miner. Process.*, 2004, **74**, S173–S181.
- <sup>27</sup> W. Morris, S. Wang, D. Cho, E. Auyeung, P. Li, O. K. Farha and C. A. Mirkin, *ACS Appl. Mater. Interfaces*, 2017, **9**, 33413–33418.
- <sup>28</sup> L. Valenzano, B. Civalleri, S. Chavan, S. Bordiga, M. H. Nilsen, S. Jakobsen, K. P. Lillerud and C. Lamberti, *Chem. Mater.*, 2011, **23**, 1700–1718.
- <sup>29</sup> L. Valenzano, B. Civalleri, S. Chavan, S. Bordiga, M. H. Nilsen, S. Jakobsen, K. P. Lillerud and C. Lamberti, *Chem. Mater.*, 2011, **23**, 1700–1718.

- <sup>30</sup> J. Rouquerol, P. Llewellyn and F. Rouquerol, *Stud. Surf. Sci. Catal.*, 2007, **160**, 40–56.
- <sup>31</sup> L. Zhou, X. Zhang and Y. Chen, *Mater. Lett.*, 2017, **197**, 167–170.
- <sup>32</sup> C. A. Clark, K. N. Heck, C. D. Powell and M. S. Wong, *ACS Sustainable Chem. Eng.*, 2019, **7**, 6619–6628.
- <sup>33</sup> A. Policicchio, M. Florent, M. F. Attia, D. C. Whitehead, J. Jagiello and T. J. Bandosz, *Adv. Mater. Interfaces*, 2020, 1902098.
- <sup>34</sup> A. J. Howarth, A. W. Peters, N. A. Vermeulen, T. C. Wang, J. T. Hupp and O. K. Farha, *Chem. Mater.*, 2017, **29**, 26–39.
- <sup>35</sup> F. X. Llabres i Xamena, and F. G. Cirujano, *J. Catal.*, 2017, **352**, 401–414.
- <sup>36</sup> J. Hajek, B. Bueken, M. Waroquier, D. De Vos and V. Van Speybroeck, *ChemCatChem*, 2017, **9**, 2203–2210.
- <sup>37</sup> D. S. Sholl and R. P. Lively, *J. Phys. Chem. Lett.*, 2015, **6**, 3437–3444.
- <sup>38</sup> M. Taddei, *Coord. Chem. Rev.*, 2017, **343**, 1–24.
- <sup>39</sup> L. Valenzano, B. Civalieri, S. Chavan, S. Bordiga, M. H. Nilsen, S. Jakobsen, K. P. Lillerud and C. Lamberti, *Chem. Mater.*, 2011, **23**, 1700–1718.
- <sup>40</sup> S. Chavan, J. G. Vitillo, D. Gianolio, O. Zavorotynska, B. Civalieri, S. Jakobsen, M. H. Nilsen, L. Valenzano, C. Lamberti, K. P. Lillerud and S. Bordiga, *Phys. Chem. Chem. Phys.*, 2012, **14**, 1614–1626.
- <sup>41</sup> O. V. Gutov, M. González Hevia, E. C. Escudero-Adán, A. Shafir, *Inorg. Chem.*, 2015, **54**, 8396–8400.
- <sup>42</sup> R. Limvorapitux, H. Chen, M. L. Mendonca, M. Liu, R. Q. Snurr, S. T. Nguyen, *Catal. Sci. Technol.*, 2019, **9**, 327–335.
- <sup>43</sup> I. V. Terekhova, E. S. Chibunova, R. S. Kumeev and G. A. Alper, *Carbohydr. Polym.*, 2014, **110**, 472–479.
- <sup>44</sup> H.-J. Schneider, F. Hacket and V. Rüdiger, *Chem. Rev.*, 1998, **98**, 1755–1785.
- <sup>45</sup> D. Prochowicz, A. Kornowicz, Iwona Justyniak and Janusz Lewiński, *Coord. Chem. Rev.*, 2016, **306**, 331–345.
- <sup>46</sup> D. Prochowicz, A. Kornowicz and J. Lewiński, *Chem. Rev.*, 2017, **117**, 22, 13461–13501.
- <sup>47</sup> J. Szejtli, *Chem. Rev.*, 1998, **98**, 1743–1753.
- <sup>48</sup> C. Hennig, S. Weiss, W. Kraus, J. Kretzschmar and A. C. Scheinost, *Inorg. Chem.*, 2017, **56**, 2473–2480.
- <sup>49</sup> M. A. Moussawi, M. Haouas, S. Floquet, W. E. Shepard, P. A. Abramov, M. N. Sokolov, V. P. Fedin, S. Cordier, A. Ponchel, E. Monflier, J. Marrot and E. Cadot, *J. Am. Chem. Soc.*, 2017, **139**, 14376–14379.
- <sup>50</sup> M. A. Moussawi, N. Leclerc-Laronze, S. Floquet, P. A. Abramov, M. N. Sokolov, S. Cordier, A. Ponchel, E. Monflier, H. Bricout, D. Landy, M. Haouas, J. Marrot and E. Cadot, *J. Am. Chem. Soc.*, 2017, **139**, 12793–12803.
- <sup>51</sup> K. I. Assaf, M. S. Ural, K. I. Assaf, M. S. Ural, F. Pan, T. Georgiev, S. Simova, K. Rissanen, D. Gabel and W. M. Nau, *Angew. Chem. Int. Ed.*, 2015, **54**, 6852–6856.
- <sup>52</sup> Y. Wu, R. Shi, Y.L. Wu, J. M. Holcroft, Z. Liu, M. Frascioni, M. H. R. Wasielewski, H. Li and J. F. Stoddart, *J. Am. Chem. Soc.*, 2015, **137**, 4111–4118.
- <sup>53</sup> A. Ryzhakov, T. D. Thi, J. Stappaerts, L. Bertoletti, K. Kimpe, A. Rodrigues Sá Couto, P. Saokham, G. Van den Mooter, P. Augustijns, G. W. Somsen, S. Kurkov, S. Inghelbrecht, A. Arien, M. I. Jimidar, K. Schrijnemakers and T. Loftsson, *J. Pharm. Sci.*, 2016, **105**, 2556–2569.
- <sup>54</sup> L. X. Song, L. Bai, X. M. Xu, J. He and S. Z. Pan, *Coord. Chem. Rev.*, 2009, **253**, 1276–1284.